Quantum Dots

Deutsche Ausgabe: DOI: 10.1002/ange.201600289
Internationale Ausgabe: DOI: 10.1002/anie.201600289

Halide–Amine Co-Passivated Indium Phosphide Colloidal Quantum Dots in Tetrahedral Shape

Kyungnam Kim[+], Dongsuk Yoo[+], Hyekyoung Choi[+], Sudarsan Tamang, Jae-Hyeon Ko, Sungwoo Kim, Yong-Hyun Kim, and Sohee Jeong**

Abstract: *Wet chemical synthesis of covalent III-V colloidal quantum dots (CQDs) has been challenging because of uncontrolled surfaces and a poor understanding of surface–ligand interactions. We report a simple acid-free approach to synthesize highly crystalline indium phosphide CQDs in the unique tetrahedral shape by using tris(dimethylamino) phosphine and indium trichloride as the phosphorus and indium precursors, dissolved in oleylamine. Our chemical analyses indicate that both the oleylamine and chloride ligands participate in the stabilization of tetrahedral-shaped InP CQDs covered with cation-rich (111) facets. Based on density functional theory calculations, we propose that fractional dangling electrons of the In-rich (111) surface could be completely passivated by three halide and one primary amine ligands per the (2 × 2) surface unit, satisfying the 8-electron rule. This halide–amine co-passivation strategy will benefit the synthesis of stable III-V CQDs with controlled surfaces.*

Wet chemistry synthesis and stabilization of ionic II-VI (CdSe, CdS) and IV-VI (PbS, PbSe) colloidal quantum dots (CQDs) have been well established experimentally over the last 30 years.[1] However, detailed understandings on the surface chemistry of the CQDs at the atomic level were limited or only recently achieved, including our own reports for IV-VI rock-salt materials.[2] The surface chemistry of CQDs for tetrahedrally coordinated II-VI and III-V compound semiconductor materials is complicated by the presence of fractional dangling electrons (DEs) on their surfaces. Based on the electron counting model,[3] there are 0.5 and 1.5 DEs per broken bond, respectively, for cation (II) and anion (VI) of II-VI materials. Similarly, there are 0.75 (III) and 1.25 (V) DEs per broken bond for III-V materials. Passivation of such fractional DEs with cationic or anionic ligands that can donate or withdraw exactly one electron is conceptually very intriguing.

Colloidal synthesis of III-V (InP, InAs) semiconducting nanocrystals is even more challenging than that of II-VI because of their additional covalency, requiring a high growth temperature in the solution chemistry and a limited choice of precursors.[4] The poorly controlled surfaces of III-V CQDs effectively limit fabrication of high quality, shape-controlled nanocrystals compared to II-VI and IV-VI CQDs.

InP CQDs are potential alternatives to toxic cadmium-based materials, and their band gaps span the entire visible range.[5] Most synthetic strategies for InP CQDs are modified version of Well's dehalosilylation reactions performed in a non-coordinating solvent, which involve fatty acids in the reaction to activate the indium precursors.[6] To produce high-quality InP CQDs with narrow size distributions, less reactive precursors have been investigated.[4a–c] However, there have been concerns about the role of fatty acids that induce surface oxidation.[7] Very recently, a non-oxygen-containing synthesis of InP CQDs was attempted.[8] Unfortunately, there have been no reports on specific shape control of InP CQDs with a detailed microscopic understanding of the underlying surface stabilization mechanism. Such information could be generally applicable for other materials.

Herein, we address, both experimentally and theoretically, the issue of III-V CQDs, that is, the unprecedented surface chemistry control of the fractional DEs of InP by using the so-called halide–amine co-passivation strategy. Our acid-free synthesis of InP nanocrystals with the co-passivation method reliably produces tetrahedrally shaped nanocrystals on a large scale, which is only enabled by the unique stabilization of indium-rich (111) facets. This co-passivation approach may serve as a guiding rule for synthesizing other III-V, and even II-VI or I-III-VI, CQDs with controlled surfaces. We were further able to epitaxially grow thick ZnS shells on tetrahedral shaped InP cores without any oxidative interface, which provide additional material stability even in harsh phase-transfer reaction.

We synthesized InP tetrahedral nanocrystals (TNCs; Figure 1), using indium trichloride ($InCl_3$) and tris(dimethylamino) phosphine ($(Me_2N)_3P$) dissolved in oleylamine, which could also serve as a coordinating ligand of TNCs, at an elevated temperature of $\geq 170\,^{\circ}C$. The growth of InP TNCs was monitored using aliquots of the reaction mixture at different times using UV/Vis spectroscopy (Supporting Information, Figure S1). The absorption maximum shifted towards longer wavelength as a function of time owing to the size increase of InP TNCs (see growth process in Figure S2),

[*] K. Kim,[+] H. Choi,[+] Dr. S. Tamang, S. Kim, Prof. S. Jeong
Nanomechanical Systems Research Division
Korea Institute of Machinery and Materials
Daejeon 34103 (Korea)
E-mail: sjeong@kimm.re.kr
D. Yoo,[+] J.-H. Ko, Prof. Y.-H. Kim
Graduate School of Nanoscience and Technology
Korea Advanced Institute of Science and Technology (KAIST)
Daejeon 34141 (Korea)
E-mail: yong.hyun.kim@kaist.ac.kr
H. Choi,[+] Prof. S. Jeong
Department of Nanomechatronics
Korea University of Science and Technology (UST)
Daejeon 34113 (Korea)
[+] These authors contributed equally to this work.

Supporting information for this article can be found under http://dx.doi.org/10.1002/anie.201600289.

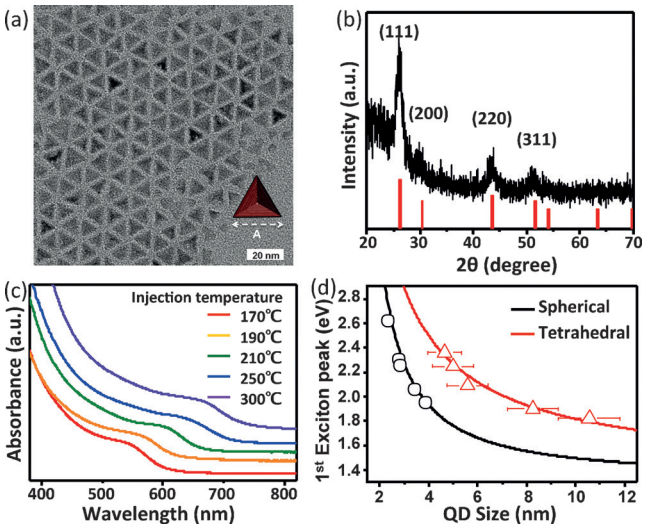

Figure 1. a) TEM image of InP tetrahedral nanocrystals (TNCs) synthesized at 300 °C. Inset: illustrated top view of a tetrahedron covered with the (111) facets. Scale bar = 20 nm. The size of the TNCs was estimated by the edge size (A) of the triangles. b) XRD pattern of InP TNCs. c) UV/Vis spectra of InP TNCs grown at various temperatures. d) The first exciton peaks as a function of CQD size for tetrahedral (present work) and spherical[9] CQDs.

clearly indicating that these TNCs are within the strong quantum confinement regime.

Figure 1 a depicts a representative transmission electron microscopy (TEM) image of strikingly aligned InP TNCs with the average edge size (A) of 10.56 ± 1.25 nm, grown at 300 °C. The inset of Figure 1 a shows the corresponding top view of a tetrahedron. In cubic symmetry crystals, the tetrahedron shape should be completely covered by the (111) facets. The X-ray diffraction (XRD) pattern of these nano-triangles corresponded to the cubic zinc blende structure of InP [JCPDF: 32-0452]. The reflections from (111) plane at 26°, (220) plane at 43°, and (311) plane at 51° were clearly visible (Figure 1 b). The TNCs were highly crystalline and directional, as manifested by the stacking sequences along the [220] direction (Figure S3). The overall size of the TNCs could be controlled by simply changing the injection temperature. Figure 1 c and Figure S4 depict, respectively, the absorbance spectra and TEM images of InP TNCs with various sizes synthesized at different injection temperatures. The triangular feature of InP particles as small as 5.0 nm (synthesized at 190 °C) was observed at high magnification (Figure S5). When the growth temperature was lower than 190 °C, TNCs could not be clearly identified (Figure S4).

Our non-spherical TNC sample was composed of a mixture of triangular prism and tetrahedron (triangular pyramid) shapes. Electron wavefunctions in tetrahedral CQDs are known to be more quantum-confined than in spherical CQDs with the same volume (Figure S6).[10] To quantify this, we compared the first exciton peaks (E_{CQD}) of InP TNCs with those of spherical CQDs as a function of CQD size (L).[9] The first exciton peaks were fitted with (Figure 1 d):

$$E_{CQD} = C/L^{\alpha} + E_{bulk} \quad (1)$$

where L is defined by the edge (A) and diameter (D) sizes, respectively, of tetrahedral and spherical CQDs. E_{bulk} is the band gap (1.35 eV) of bulk InP, and C and α are fitting parameters (Table 1). From the effective mass theory of the finite-potential-well problems, one can easily obtain α = 2.[10] For quantum dots, however, α is typically smaller than 2,[9] indicating that the electron–electron correlation leads to stronger electron confinement than in the simplest theory. The fitting formula in [Eq. (1)] shall be used to estimate the CQD size from the optical measurement.

Table 1: Obtained fitting parameters for the first exciton peaks of tetrahedral and spherical CQDs.[a]

	C	α
Tetrahedral CQDs	4.25	0.96
Spherical CQDs	4.28	1.47

[a] E_{bulk} = 1.35 eV was used.

The InP TNCs are In-rich, with an In/P ratio of 1.15–1.31 as confirmed from inductively coupled plasma (ICP) analysis (Table S1). Therefore, we speculated that well-dispersed InP TNCs are covered with four indium-rich (111) facets, in which a portion of surface In atoms must be coordinated with oleylamine ligands.

To confirm this, we further investigated the microscopic chemical structure of InP TNCs. Figure 2 indicates that both the chloride and oleylamine ligands passivate the indium-rich (111) facets of InP TNCs, as characterized with X-ray photoelectron spectroscopy (XPS) and nuclear magnetic resonance (NMR).[2,11] In the XPS data, both chlorine (Cl) and nitrogen (N) atoms were detected (Figure 3a, b). The measured Cl 2p 3/2 binding energy (198 eV) for TNCs is down-shifted by 1.1 eV in reference to the starting materials, $InCl_3$ (199.1 eV), indicating that Cl closely interacts with InP

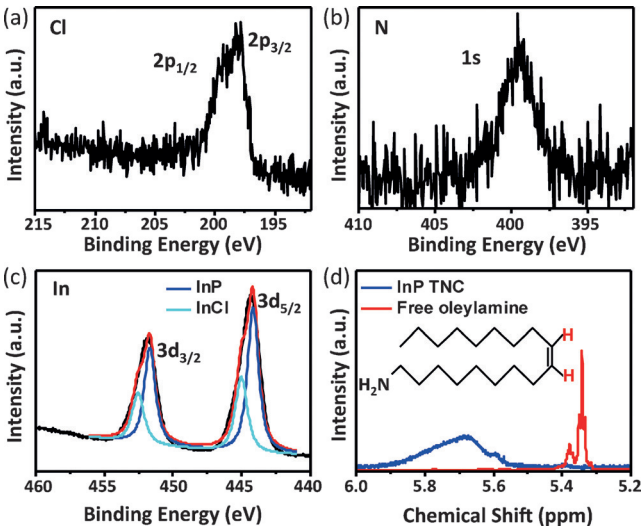

Figure 2. High-resolution XPS spectra of InP TNCs. XPS spectra of a) Cl 2p, b) N 1s, and c) In 3d. The In peaks were deconvoluted with InP and InCl subpeaks. d) 1H NMR spectra of InP TNCs capped with oleylamine (blue) and free oleylamine (red) in [D_6]benzene.

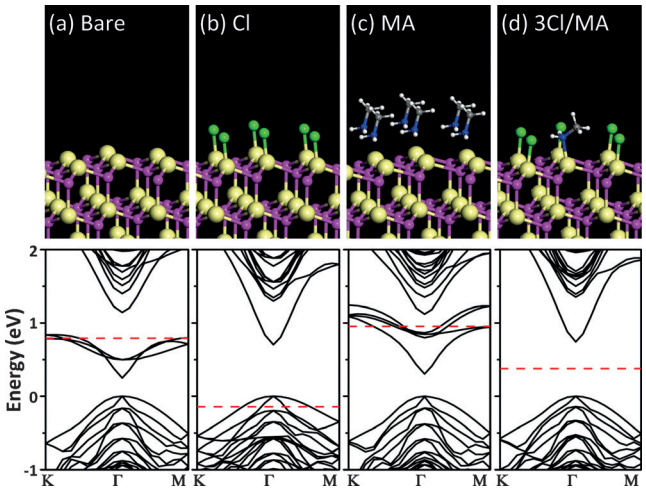

Figure 3. Side views of ball-and-stick models of a) bare, b) Cl-passivated, c) methylamine (MA)-passivated, and d) 3 Cl:1 MA (molar ratio)-passivated indium-rich (111) InP surfaces (yellow: In, magenta: P, green: Cl, blue: N, grey: C, and white: H) and their respective band structures near the Fermi energy, marked by the dashed red line. The valence band maximum is set to energy zero. A clear band gap opening in (d) indicates the perfect passivation of the polar (111) surface.

TNCs.[12] Also, the measured N 1s binding energy is 399.3 eV, which is noticeably higher than that of typical primary amines (398 eV).[13] This implies that the lone-pair electrons of primary amines strongly couple with the TNC (111) facets. By integrating the Cl 2p and N 1s peaks, we obtained the Cl/N composition ratio of ≈ 1 (Table S2). Figure 2c shows XPS counts from In 3d electrons. In 3d 5/2 and 3/2 electrons have their binding energies at 444 and 452 eV, respectively, which mostly correspond to InP bulk.[14] The In peaks broaden to the high binding energy region (444.3–447.0 eV and 451.8–454.6 eV), which results from chloride passivation (In-Cl) on InP surfaces.[12,15] To more clearly confirm that oleylamine interacts with InP TNCs, we measured the NMR chemical shifts of the alkene protons in the range 6.0–5.2 ppm (Figure 2d). The resonances of oleylamine with InP TNCs showed broadening and a downfield shift relative to free oleylamine, which are features generally observed when the ligands interact with nanoparticles.[16] NMR ligand quantification[17] indicated that the oleylamine ligand coverage of InP CQDs grown at 300 °C was 1.55 nm^{-2} (Table S3).

To understand, microscopically, how the indium-rich (111) facet is stabilized with chloride and oleylamine during the formation of InP TNCs, we performed first-principles density-functional theory (DFT) calculations (Supporting Information) for indium-terminated InP (111) surfaces under various passivation conditions with chloride and methylamine (MA; Figure 3). The bare unpassivated (111) surface showed the metallic character, indicating that it is highly unstable, or very reactive. Every In atom on the surface has 0.75 DEs, requiring 1.25 electrons for passivation, according to the electron counting model.[3] When we passivated the (111) surface with chlorine atoms, we could see a tight bond between surface In and Cl, with a formation energy of −2 eV per Cl (Table S4), and a removal of DE states at the band gap region. However, because Cl can provide only one electron when coordinating with surface In, the chlorine-passivated surface was still electron-deficient (Figure 3b). When we coordinated MA onto the surface, the binding energy was almost negligible (0.12 eV per MA). Chemical bonds did not form, nor were DE states removed (Figure 3c). For the perfect passivation of the 0.75 DEs, we would need three Cl atoms and one MA molecule to be coordinated to the (2 × 2) surface unit (Figure 3d; Supporting Information, Figure S7). For the (2 × 2) surface model, three electrons from three Cl atoms and two lone-pair electrons from the amine group co-passivate three DEs from four surface In atoms, satisfying the 8-electron rule per (2 × 2) unit cell. The theoretical MA coverage is 1.7 nm^{-2}, and the MA binds datively to the surface In atom, with a binding energy of about 1.8 eV per MA (Figure S8).

The above theoretical consideration suggests a route for perfect passivation of cation-rich (111) surfaces with fractional DEs by employing the so-called halide–amine co-passivation method, which can be easily generalized for other materials. Note that the experimental amine coverage is very close to the theoretical value. Our current approach, however, needs to be further optimized for perfect passivation, as the experimental halide–amine ratio (≈ 1) deviates from the ideal value of 3:1.

Creating a thick shell of ZnS over InP CQDs has been difficult in acid-containing reactions.[18] Therefore, we again used acid-free precursors, namely, $ZnCl_2$ and 1-dodecanethiol as Zn and S precursors, respectively, for ZnS shell formation onto our well-defined tetrahedral InP core by successive ion layer adsorption. The core/shell structure retained the tetrahedral shape of the core (Figure 4a). The size of the core/shell TNCs, determined by measuring the edge size of the TNCs (Figure S9), were found to be 15.04 ± 2.8 nm, about 10 nm larger than the mean core size (≈ 5.8 nm), which was estimated by the first absorption peak position (at 580 nm) and [Eq. (1)] of TNCs.[5] The size difference can be used for estimating the face-to-face shell thickness of core–shell TNCs

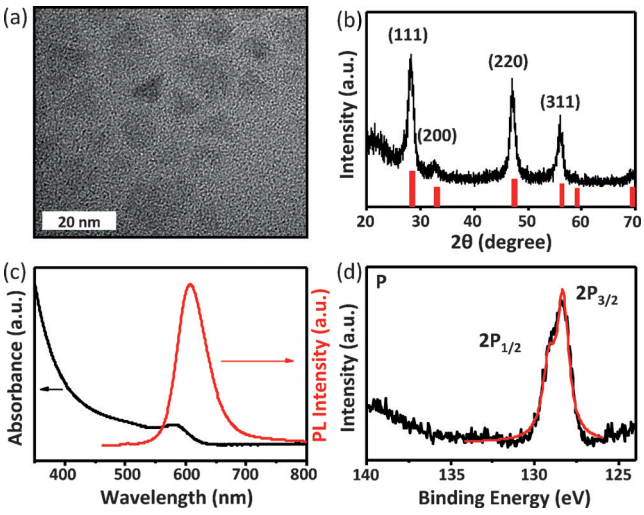

Figure 4. a) TEM image, b) XRD patterns, c) absorbance and PL spectra, and d) P 2p XPS spectrum of InP/ZnS core/shell TNCs grown at 250 °C. Scale bar = 20 nm.

following the formula $(A-A')/\sqrt{24}$, where A and A′ are edge sizes of core–shell and core, respectively. The estimated shell thickness is then 1.9 nm. Conventional synthesis of InP/ZnS NCs using fatty acids typically results in very thin shell thickness (< 1 nm).[18] While the shell thickness varies with the core size, we can typically grow over 15-nm-sized TNCs retaining the shape from the 5 nm TNC starting cores, which represents a ZnS shell of up to 2 nm thickness. Thicker shell formation above 2 nm often causes aggregation and changes in shape (Figure S10). The successful formation of the InP/ZnS core/shell, as observed in TEM, was confirmed by XRD pattern (Figure 4b). The diffraction patterns from cubic ZnS shell were clearly detected [JCPDF card 05-0566]. Previous reports on the XRD pattern of InP/ZnS core/shell CQDs suggested that the diffraction peaks locate in the middle position of InP and ZnS owing to the thin shell.[19] In our case, because of the very thick shell, only the ZnS peaks are visible. These epitaxially grown core/shell TNCs with large shell thickness were highly luminescent (Figure 4c), while the InP core showed only surface trap emission (Figure S11).

Fatty acids are known to undergo thermal degradation at high temperature, thereby contributing to the surface oxidation of InP.[7] Virieux et al. reported that InP CQDs naturally formed an oxide phase at the interface under traditional synthetic condition using fatty acids. This was confirmed from the observed XPS binding energy around 133 eV in the P 2p spectrum, which was attributed to the oxide phase of $InPO_x$.[7b] Our overall reaction does not involve any fatty-acid- or oxygen-containing ligands. XPS studies indeed indicated that there is no interfacial oxidation in the InP/ZnS core–shell TNCs (Figure 4d). For a better understanding, InP TNC cores were exposed to air prior to shell growth. Interestingly, the tetrahedral shape was not retained in InP/ZnS core–shell nanocrystals (Figure S12). These core/shell nanocrystals had the characteristic oxide signature around 133 eV (Figure S12c), similar to the ones observed for spherical InP/ZnS CQDs synthesized using fatty acids (Figure S13b). Therefore, the oxide-free environment is necessary for the successful growth of a thick ZnS shell, and the resultant tetrahedral shape of the core may additionally affect the epitaxial formation of a thick shell on (111) facets.

The thick shell over the core is expected to render high stability. Encouraged by the TEM results, we tested the beneficial role of these robust InP/ZnS TNCs under the extremely adverse conditions prevalent in phase transfer reactions. Phase transfer of typical InP/ZnS CQDs using thiol-containing ligands results in dramatic quenching of photoluminescence (PL), attributed to thin shell thickness.[20] The InP/ZnS TNCs, with different core sizes and shell thicknesses (Table S5), were transferred to aqueous medium using thioglycolic acid (TGA) as the phase-transferring agent in basic media (pH 10). The TGA treatment time was 2 h. The absolute quantum yield (QY) of TGA capped sample in aqueous medium was compared with corresponding CQDs in organic medium at different shell thicknesses (Table S5). QY of InP/ZnS TNCs with the thinner shell decreased more than with the thicker shell. As much as 60% of the initial QY (47%) was retained in TGA-treated CQDs coated with thick ZnS shells of 1.4 nm (Figure S14).

In conclusion, we synthesized tetrahedrally shaped InP nanocrystals in a colloidal form by reacting $InCl_3$ and $(Me_2N)_3P$ in oleylamine. The resulting tetrahedral InP nanocrystals are covered with indium-rich (111) facets passivated by both the chloride and primary amine ligands. These co-passivated tetrahedral nanocrystals showed strong deviation from their spherical counterparts with regards to the quantum confinement and shell growth. The halide–amine copassivation method would be useful for stabilizing high-quality shape-controlled III-V CQDs.

Acknowledgements

This work was supported by the Global Frontier R&D program by the Center for Multiscale Energy Systems (2011-0031566), the Global R&D program (1415134409) funded by KIAT, and KIMM research grant (NK196E). S.T. was on study leave from Skimm University. Work at KAIST was supported by the NRF (2015R1A2A2A05027766).

Keywords: colloidal quantum dots · co-passivation · halides · indium phosphide · tetrahedral shape

How to cite: *Angew. Chem. Int. Ed.* **2016**, *55*, 3714–3718
Angew. Chem. **2016**, *128*, 3778–3782

[1] a) C. B. Murray, D. J. Norris, M. G. Bawendi, *J. Am. Chem. Soc.* **1993**, *115*, 8706–8715; b) C. B. Murray, C. R. Kagan, M. G. Bawendi, *Annu. Rev. Mater. Sci.* **2000**, *30*, 545–610; c) M. A. Hines, G. D. Scholes, *Adv. Mater.* **2003**, *15*, 1844–1849; d) R. Costi, A. E. Saunders, U. Banin, *Angew. Chem. Int. Ed.* **2010**, *49*, 4878–4897; *Angew. Chem.* **2010**, *122*, 4996–5016.

[2] a) H. Choi, J.-H. Ko, Y.-H. Kim, S. Jeong, *J. Am. Chem. Soc.* **2013**, *135*, 5278–5281; b) J. Y. Woo, J.-H. Ko, J. H. Song, K. Kim, H. Choi, Y.-H. Kim, D. C. Lee, S. Jeong, *J. Am. Chem. Soc.* **2014**, *136*, 8883–8886.

[3] Y.-H. Kim, M. J. Heben, S. B. Zhang, *Phys. Rev. Lett.* **2004**, *92*, 176102.

[4] a) D. Franke, D. K. Harris, L. Xie, K. F. Jensen, M. G. Bawendi, *Angew. Chem. Int. Ed.* **2015**, *54*, 14299–14303; *Angew. Chem.* **2015**, *127*, 14507–14511; b) S. Joung, S. Yoon, C.-S. Han, Y. Kim, S. Jeong, *Nanoscale Res. Lett.* **2012**, *7*, 1–8; c) D. K. Harris, M. G. Bawendi, *J. Am. Chem. Soc.* **2012**, *134*, 20211–20213; d) D. C. Gary, B. A. Glassy, B. M. Cossairt, *Chem. Mater.* **2014**, *26*, 1734–1744; e) D. C. Gary, M. W. Terban, S. J. L. Billinge, B. M. Cossairt, *Chem. Mater.* **2015**, *27*, 1432–1441.

[5] a) O. I. Mićić, H. M. Cheong, H. Fu, A. Zunger, J. R. Sprague, A. Mascarenhas, A. J. Nozik, *J. Phys. Chem. B* **1997**, *101*, 4904–4912; b) L. Li, M. Protière, P. Reiss, *Chem. Mater.* **2008**, *20*, 2621–2623; c) X. Wang, L. Qu, J. Zhang, X. Peng, M. Xiao, *Nano Lett.* **2003**, *3*, 1103–1106.

[6] R. L. Wells, A. T. McPhail, L. J. Jones, M. F. Self, *Polyhedron* **1993**, *12*, 141–147.

[7] a) K. Huang, R. Demadrille, M. G. Silly, F. Sirotti, P. Reiss, O. Renault, *ACS Nano* **2010**, *4*, 4799–4805; b) H. Virieux, M. Troedec, A. Cros-Gagneux, W.-S. Ojo, F. Delpech, C. Nayral, H. Martinez, B. Chaudret, *J. Am. Chem. Soc.* **2012**, *134*, 19701–19708; c) L. Xie, D. K. Harris, M. G. Bawendi, K. F. Jensen, *Chem. Mater.* **2015**, *27*, 5058–5063.

[8] a) W.-S. Song, H.-S. Lee, J. C. Lee, D. S. Jang, Y. Choi, M. Choi, H. Yang, *J. Nanopart. Res.* **2013**, *15*, 1–10; b) M. D. Tessier, D. Dupont, K. D. Nolf, R. D. Roo, Z. Hens, *Chem. Mater.* **2015**, *27*, 4893–4898.

[9] a) K. Kim, C.-S. Han, S. Jeong, *J. Mater. Chem.* **2012**, *22*, 21370 – 21372; b) E. Cho, H. Jang, J. Lee, E. Jang, *Nanotechnology* **2013**, *24*, 215201.
[10] W.-K. Li, S. M. Blinder, *Chem. Phys. Lett.* **2010**, *496*, 339 – 340.
[11] T. G. Kim, H. Choi, S. Jeong, J. W. Kim, *J. Phys. Chem. C* **2014**, *118*, 27884 – 27889.
[12] B. H. Freeland, J. J. Habeeb, D. G. Tuck, *Can. J. Chem.* **1977**, *55*, 1527 – 1532.
[13] J. F. Moulder, W. Stickle, P. E. Sobol, K. D. Bomben, *Handbook of X-ray Photoelectron Spectroscopy*, Physical Electronics, Eden Prairie, **1995**.
[14] M. Faur, M. Faur, D. T. Jayne, M. Goradia, C. Goradia, *Surf. Interface Anal.* **1990**, *15*, 641 – 650.
[15] J. H. Thomas, G. Kaganowicz, J. W. X. Robinson, *J. Electrochem. Soc.* **1988**, *135*, 1201 – 1206.
[16] Z. Hens, J. C. Martins, *Chem. Mater.* **2013**, *25*, 1211 – 1221.
[17] N. C. Anderson, M. P. Hendricks, J. J. Choi, J. S. Owen, *J. Am. Chem. Soc.* **2013**, *135*, 18536 – 18548.
[18] a) S. Kim, T. Kim, M. Kang, S. K. Kwak, T. W. Yoo, L. S. Park, I. Yang, S. Hwang, J. E. Lee, S. K. Kim, S.-W. Kim, *J. Am. Chem. Soc.* **2012**, *134*, 3804 – 3809; b) K. Kim, H. Lee, J. Ahn, S. Jeong, *Appl. Phys. Lett.* **2012**, *101*, 073107; c) X. Yang, D. Zhao, K. S. Leck, S. T. Tan, Y. X. Tang, J. Zhao, H. V. Demir, X. W. Sun, *Adv. Mater.* **2012**, *24*, 4180 – 4185.
[19] a) P. Reiss, M. Protière, L. Li, *Small* **2009**, *5*, 154 – 168; b) S. Hussain, N. Won, H. Jin, H. Chung, S. Kim, *ChemPhysChem* **2009**, *10*, 1466 – 1470.
[20] S. Tamang, G. Beaune, I. Texier, P. Reiss, *ACS Nano* **2011**, *5*, 9392 – 9402.

Received: January 11, 2016
Published online: February 5, 2016

